ALPHA FOUNDATION FOR THE IMPROVEMENT OF MINE SAFETY AND HEALTH

Final Technical Report

Project Title: Advanced Low Noise Fan Array System

Grant Number: AFC215FO-71

Organization: Mechanical Engineering Department - Virginia Polytechnic Institute and State University

Principal Investigator: Prof. Ricardo A. Burdisso
Contact Information : Email Address: rburdiss@vt.edu
Phone Number: 540-231-7355

Administrative Contact: Nevada Davis, MBA, CRA
Contact Information : Email Address : ngdean@vt.edu
Phone Number: 540-231-6653

Period of Performance: August 2018-September 2019

Acknowledgement/Disclaimer: This study was sponsored by the Alpha Foundation for the Improvement of Mine Safety and Health, Inc. (ALPHA FOUNDATION). The views, opinions and recommendations expressed herein are solely those of the authors and do not imply any endorsement by the ALPHA FOUNDATION, its Directors and staff.

1. Executive Summary:

According to the National Institute for Occupational Safety and Health (NIOSH), poor air quality due to insufficient air flow and accumulated air contaminants can create a hazardous working environment for exposed workers. Physical hazardous agents that mine workers are exposed to on a daily basis include among others noise, vibration, temperature, and dust. When these conditions exist, the use of ventilation fans is necessary to provide a healthful and safe working environment. However, for ventilation fans to be effective, they need to be in close proximity to the working areas. Consequently, loud ventilation fans are one of the most harmful sources of noise due to their proximity to the workers. Long term exposure to harmful noise levels can lead to irreversible hearing damage, i.e. noise-induced hearing loss (NIHL). According to NIOSH ***noise is one of the greatest hazards to a miner's health, rivaled only by respirable dust and repetitive trauma*** (Matetic et al., 2012). Thus, there is still a pressing need to reduce the exposure of miners to noise. If the Permissible Exposure Level (PEL) is exceeded, the mine operator is required to use all feasible engineering and/or administrative controls to reduce miner's exposure. This is not trivial problem as there are several noise sources in a mining operation that can contribute to this challenge. Ventilation fans are one of the most dominant noise sources and thus a prime target for noise control and mitigation. In fact, ventilation fans are the second loudest noise source in coal mine operations(Cherniack et al., 2012). This ventilation fan noise problem is not unique to the mine operations, and is very common through many other industries.

The main premise of this work is that reducing the fan speed while maintaining a high aerodynamic efficiency will result in significant noise reduction. This approach is justified considering that the fan aerodynamic noise scales directly with the 4-6th power of the fan speed, i.e. reducing the speed by half can reduce noise levels by up to 18 dB. To this end, the approach here is to improve the aerodynamic characteristics of the blades to reduce the fan speed and noise while maintaining a high aerodynamic efficiency. Therefore, a control vortex design (CVD) approach for the design of the blades was implemented to improve the contributions of the blade sections at higher radii (Burdisso et al., 2017; Hurtado and Burdisso, 2018), i.e. axial flow velocity increases from the fan hub to the tip. The CVD approach was developed as part of a previous project (Alpha Foundation award number AFC215-21).

As part of the current research effort, an advanced fan array system was developed, fabricated and tested. Figure 1 shows front and back views of the 7-fans array. All fans have the same blade geometry driven by individual motors. The multi-element fan has been implemented into the fan array concept shown hereafter referred to as the VTFA (**V**irginia **T**ech **F**an **A**rray) unit. Multi-element airfoils are implemented in the design of the blades for the fan to further improve the aerodynamic characteristics of the blades and enable lower fan speeds and noise. Figure 2 shows a single fan with the multi-element blade. Multi-element airfoil configurations outperform single element airfoils by operating at higher lift conditions while preventing flow separation and subsequent stall. To the best of the author's knowledge, this is the first implementation of multi-element airfoils for the design of low speed portable axial flow fans. The diameter of the fan in Figure 2 is 186 mm (7.3") and it operates at a tip speed of 0.105 Mach.

(a) (b)

Figure 1: Multi-fan array design (a) front and (b) rear view.

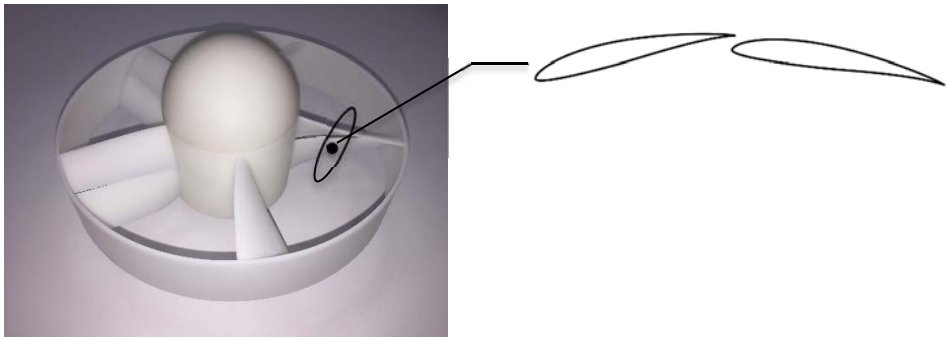

Figure 2: Multi-element fan design.

In Figure 3, the new VTFA multi-fan design is compared to commercial fans in terms of overall sound power level in dBA and volumetric flow rate in CFM. In addition, the size of the data circles is proportional to the diameter of the fan. The diameter of selected fans is noted in the figure. The commercial fan data was collected from published manufactured data. This information was taken at face value and, thus, its accuracy not independently assessed. The only exemption is the baseline Cincinnati fan used as the baseline case whose performance was measured at Virginia Tech as part of award AFC215-21 (Burdisso et al., 2017).

Since the sound power level is used in this report as the main metric to assess noise performance, it is important to explain in layman's terms the relationship between sound pressure and sound power levels. The acoustic energy emitted by a sound source is perceived by humans as pressure fluctuations at the ears (noise). The magnitude of the pressure fluctuations is quantified as "sound pressure level (SPL)" in decibels, e.g. 80 dBA indicates how loud the source is perceived by a person. The higher the level the louder the source is. The closer a person is to a noise source, the louder the source gets and the higher the sound pressure level. Thus, the sound pressure level of a source depends on the distance to the source. To characterize how loud a source is independent of the distance to it, a different metric is used: the "sound power level" also measured in decibels.

Physically, the sound power level of a source indicates the total amount of acoustic energy emitted by the source independent of distance and direction. Important to note is that the sound pressure level at a certain distance is estimated from the sound power level and the ambient conditions. Thus, in engineering practice sound power level is the correct metric used to compare different sound sources. A useful analogy to understand this concept is the relationship between the power of a heater (in watts) and the temperature (in degrees) it produces. If you are close to the heater, you feel heat from it experienced as temperature while the power remains the same (independent of distance). As you move away, the temperature will drop. Thus, the heater power and temperature are equivalent to sound power and pressure level.

As illustrated in Figure 3, the VTFA (green circle) generates a volumetric flow rate of 6626 CFM with 5 fans operating at 3000 rpm while generating 81.7 dBA overall sound power level. The VTFA unit outperforms all commercial fans of smaller sizes. Specifically compared to the baseline Cincinnati fan, the VTFA fan produces nearly the same flow rate (6626 vs 7311 CFM) at much lower noise levels (81.7 vs 98.3 dBA), e.g. a 16.6 dB reduction. Though several VTFA unit configurations were tested (number of operating fans and rpms), the one presented here (green circle) is the best in terms of both noise and flow rate. For completeness, the single fan (shown as red circle) design used in the VTFA system as tested in the anechoic chamber is also shown in this figure. It can be observed that this fan outperforms all other fan except for one. However, the diameter of this fan (0.32 m) is nearly twice the size of the single fan (0.18 m). Additional details are provided in the rest of the report.

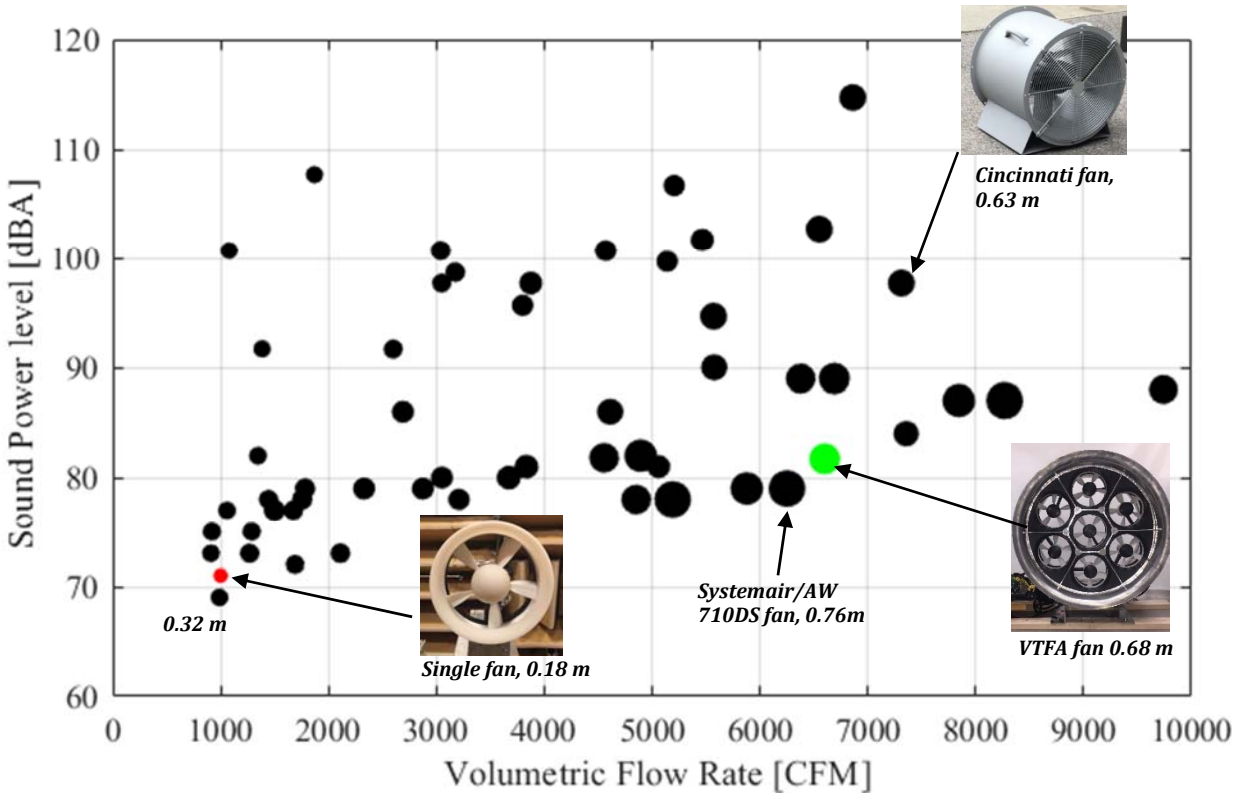

Figure 3: Performance of VTFA fan compared to commercial fans.

More insight into the system acoustic performance is determined by inspecting the narrowband sound power spectrum as shown in Figure 4. In this figure, the measured narrowband acoustic power spectrum for the VTFA unit and for the baseline Cincinnati fan are shown. Firstly, the VTFA unit produces significantly less noise (10 to 20 dB) over the whole frequency range of interest (100 to 20000 Hz). The noise from the motor is visible in the tones at high frequency (7 to 10 kHz) and it has nearly insignificant contribution to the overall noise level. In the previous program (award AFC215-21 – Burdisso et al., 2017), it was found that the noise from the motor was a significant source. Thus, the design of the VTFA involved the selection of quiet drivers for fan as it is discussed later in the report. Secondly, the VTFA unit has a dominant hay-stack peak at slightly above 1000 Hz. It was determined that this was mechanical noise resulting from vibration of the fan cylindrical casing. Though this noise component doesn't contribute much to the overall levels, it can be eliminated by some standard vibration control techniques such as better balancing of the fans (dynamics vs static), adding structural damping, structural redesign to shift resonances, and so forth. Finally, it can be observed that the VTFA unit do not shows any blade passage frequency (BPF) tones typical of fans. For example, the Cincinnati fan shows tones at the BPF (~ 180 Hz) and its harmonics. The reason that the VTFA doesn't have the BPF and harmonic tones is that the individual fans were operated all at slightly different fan speeds (approximately +/- 10 rpm) thus eliminating the constructive interference between the fans at the BPF tones, e.g. acoustic energy was scattered out over a range of frequencies rather than a single frequency.

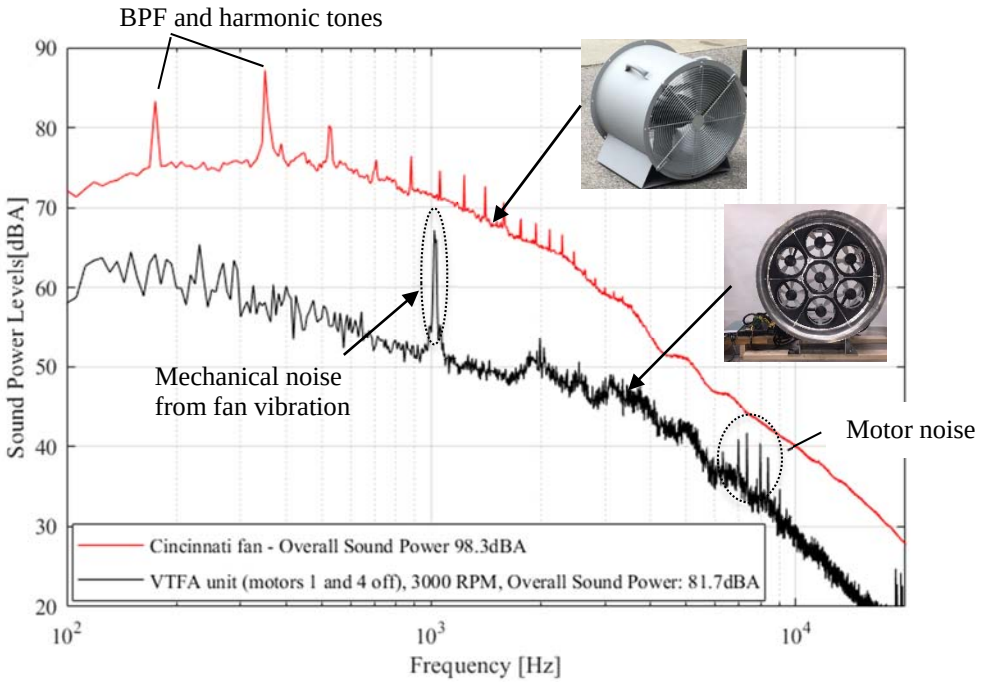

Figure 4: Narrow band sound power spectrum for the VTFA unit (all fans on) vs the baseline Cincinnati fan.

In summary, the most important conclusion from the two projects (AFC215-21 and AFC215FO-71) is that it is completely feasible to design quiet, compact and efficient ventilation fans. In fact, it can be virtually guaranteed that fans with the innovations investigated in these programs will provide

at a minimum 15 dB quieter operation than the “typical” commercial fan. This noise reduction will clearly improve the health and safety of workers, not only in the mining field, but in all industries that regularly uses ventilation fans.

The original goal was to experimentally demonstrate > 25 dB noise reduction relative to the baseline Cincinnati fan with similar flow performance and size. The 25 dB reduction was a very aggressive goal that it was not accomplished (best achieved reduction was 16.6 dB). From Figure 3, the VTFA unit outperformed the commercial fans, i.e. fans that produce more volumetric flow rate are louder while quieter fans produce less volumetric flow rate. It is worth to mention that there are other commercial fans that are very close in performance to the VTFA unit. The closest one is the Systemair/AW 710 DS fan with a diameter of 0.763 m, generating a volumetric flow rate of 6250 CFM, and producing 79 dBA of sound power level. This fan had the largest diameter of all commercial units.

In spite of not meeting the noise reduction goal, the project was successful in other aspects. Briefly, i) a new optimized design approach for low-pressure axial ventilation fans considering both aerodynamic performance and aerodynamic noise has been developed, ii) the first implementation of multi-element airfoils in the design of low-pressure axial ventilation fan blades in the open literature was demonstrated, and iii) a new multi-fan unit concept was designed and experimentally tested.

2. Problem Statement and Objective:

2.1 Problem Statement

Physical hazardous agents that mine workers are exposed to on a daily basis include among others noise, vibration, temperature, and dust. Noise--induced hearing loss is a critical issue for the mine workforce. According to NIOSH noise is one of the greatest hazards to a miner's health, rivaled only by respirable dust and repetitive trauma (Matetic et al., 2012). Thus, there is still a pressing need to reduce the exposure of miners to noise. If the Permissible Exposure Level (PEL) is exceeded, the mine operator is required to use all feasible engineering and/or administrative controls to reduce miner's exposure. This is not trivial problem as there are several noise sources in a mining operation that can contribute to this challenge. Ventilation fans are one of the most dominant noise sources and thus a prime target for noise control and mitigation. In fact, ventilation fans are the second loudest noise source in coal mine operations (Cherniack et al., 2012). Ventilation systems must provide air to all places in an underground mine to maintain a safe level of oxygen, dilute and remove noxious gases, control airborne dust, and, control temperature and humidity in the working areas. The primary ventilation system for underground mines consists of a very large surface fan pumping air and distributing it through the mine. Temporarily mounted auxiliary ventilation fans are also used to supplement the air to specific working areas. These fans are much smaller than the primary one. However, these auxiliary fans are in close proximity to the miners and thus have a more detrimental impact on the workers. This ventilation fan noise problem is not unique to the mine operations, and is very common through many other industries.

2.2 Problem Objectives

The main aim of this project is to experimentally demonstrate a novel quiet ventilation fan unit. To this end, new fan design innovations have been implements to reduce fan noise. They are:

1. Optimized fan design based on the control vortex design (CVD) approach.
2. Multi-element airfoils for the design of the blades.
3. A fan-array unit concept (7 fans).
4. Quiet BLDC motors to drive the fans.

It is important to mention that it was established as an objective target to experimentally demonstrate > 25 dB noise reduction relative to the baseline Cincinnati fan with similar flow performance. This was a very aggressive goal that it was not accomplished with the best measured reduction at 16.6 dB.

3. Research Approach:

The main premise of this research effort is that reducing the fan speed will result in significant noise reductions. This approach is justified considering that the fan aerodynamic noise scales directly with the 4-6th power of the fan speed. To this end, the approach here is to improve the aerodynamic characteristics of the blades to reduce the fan speed and noise while maintaining a high aerodynamic efficiency. Therefore, a control vortex design (CVD) approach for the design of the blades was implemented to improve the contributions of the blade sections at higher radii, i.e. axial flow velocity increases from the fan hub to the tip. Additionally, multi-element airfoils are implemented in the design of the blades to further improve the aerodynamic characteristics of the blades and enable lower fan speeds and noise. Therefore, the design of the multi-element fan is the

main focus of phase 1 of the research effort. Phase 1 is presented in section 3.1. The fan design is then incorporated into an array of 7 fans (VTFA unit) as part of phase 2 of this research effort. The design and experimental validation of the VTFA unit is described in Section 3.2.

3.1 Phase 1: Multi-element fan design

In this section, a single fan is designed incorporating multi-element airfoil blades to enable lower fan speeds and noise. The fan design has been fabricated and experimentally validated as part of phase 1 of this research effort.

Design of multi-element airfoil

A multi-element airfoil consists of closely coupling two or more single airfoils as illustrated in Figure 5 where 2 single airfoils are used (2-element airfoil). The design of a multi-element airfoil implies to select the profile of the individual airfoils, the number of elements, and their relative position. In the work here, two constrains were imposed in the design of the multi-element airfoil. Firstly, the airfoil profile is limited to the E214 airfoil given its proven superior characteristics at low speeds relative to other single element airfoils. Secondly, the number of elements is limited to two. Hence, hereafter the multi-element airfoil will be simply referred to as a tandem airfoil. The design parameters considered for the design of the tandem airfoil are shown in Figure 5. They are the chord ratio ($c2/c1$), airfoil angles ($\delta_1$and δ_2), gap size (defined when $\delta_1 = \delta_2 = 0$) and vertical position of the rear element (d_{TE}). The optimization of the airfoil configuration is conducted at a chord Reynolds number of 200,000 ($RE_t = c_{total} V_{rel} / \nu$) using the viscous/inviscid MSES/MSIS code (Drela, 2007). The design of the tandem airfoil were guided by the following objectives: (1) to achieve high lift without significantly decreasing the drag-to-lift ratio and (2) to have configuration that can be fabricated, e.g. gap between two airfoils must be large enough to allow for fabrication using 3D printing technology. The geometric and aerodynamic characteristics of the best airfoil geometry resulting from the optimization process is shown in Table 1.

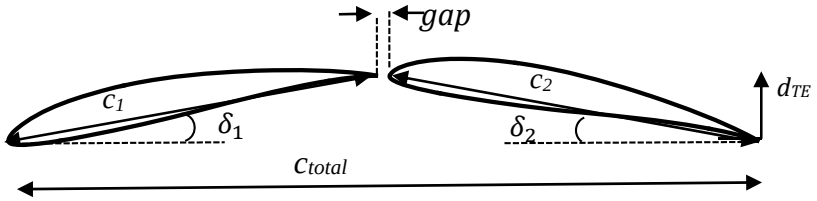

Figure 5: Design parameters for the tandem airfoil geometry.

Table 1: Geometric and aerodynamic characteristics of the tandem airfoil design.

Parameter	
Airfoil geometry	E214 airfoil
c_2 / c_1	1.0536
Leading airfoil angle (δ_1)	12 deg.
Trailing airfoil angle (δ_2)	9.28 deg.
Gap size	0.0
d_{TE}	-2% of the total chord
Maximum lift coefficient	1.95
Maximum lift to drag ratio	87.9

The coefficient of lift and drag of the tandem airfoil are compared to a single element airfoil in Figure 6. Here it can be illustrated that the tandem airfoil results in a significant increase of the lift coefficient from ~1.2 to ~1.95 (Figure 6a) while there is also an increase in the drag from ~ 0.01 to ~0.015 (Figure 6b). However, a plot of the lift to drag ratio as a function of the lift coefficient in Figure 7 illustrates better the improved aerodynamic performance of the tandem airfoil. This figure reveals that the tandem airfoil has increased the lift while keeping the same lift to drag ratio. Table 2 presents a comparison of the single and tandem airfoil at their maximum lift to drag ratio of 87.9.

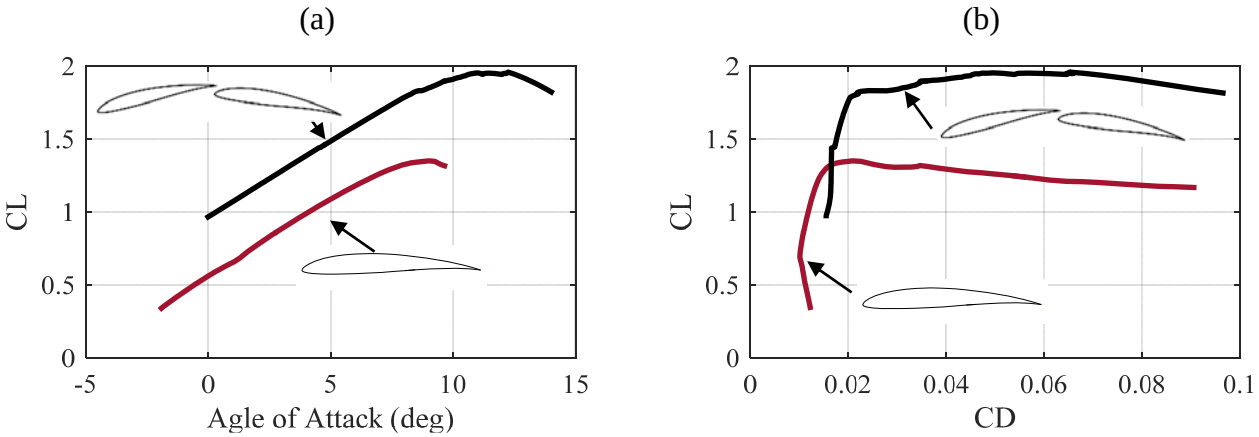

Figure 6: (a) Lift coefficient vs AoA and (b) lift vs drag coefficients for the tandem and single element airfoil for a chord Reynolds number of 200,000.

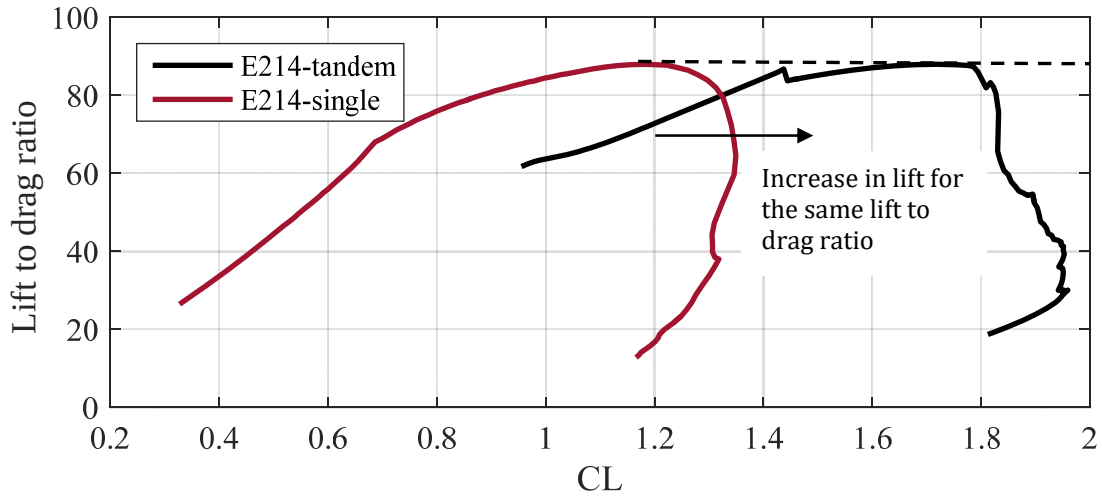

Figure 7: Lift to drag ratio vs lift coefficient for the tandem and single element airfoil for a chord Reynolds number of 200,000.

Table 2: Tandem and single element airfoil characteristics at the maximum lift to drag ratio of 87.9.

Airfoil	AoA	CL	CD
E214-airfoil	6	1.179	0.01341
Tandem airfoil	7.4	1.727	0.01964

Fan Design

The single fan has been designed to generate a target volumetric flow rate of 1030 CFM, i.e. 7200 CFM for 7 fans. To this end, a multi-objective Genetic Algorithm (GA) optimization has been implemented to design the velocity profile that satisfies the volumetric flow rate requirement. Next, an inverse design is implemented that uses the classical blade-element/vortex formulation to design the blade geometry that results in the desired velocity profiles.

The design of the velocity profile involves finding the hub-to-tip ratio ($v = r_h / r_t$) and the tip tangential velocity (M_{tan}) that result in the target volumetric flow rate. The tip tangential velocity is

$$M_{\tan} = \Omega r_t / c_{air} \qquad \textbf{(3.1)}$$

where Ω is the angular velocity, r_t is the tip radius, r_h is the hub radius, and c_{air} is the speed of sound.

Additionally, the velocity distribution is also an important parameter as it can be used to further improve the aerodynamic characteristics of the blades. To this end, the velocity profile is designed to increase from the hub to the tip while maintaining radial equilibrium using the control vortex design methodology presented under award AFC215-21(Burdisso et al., 2017). Here, radial equilibrium is incorporated into the design of the velocity profile by solving the radial equilibrium equation assuming a swirl velocity power law distribution defined as

$$v_\theta(r) = ar^n \qquad \textbf{(3.2)}$$

where a is the swirl velocity coefficient and n is the swirl velocity exponent. The resulting axial velocity distribution that maintains radial equilibrium is

$$v_a(r) = \sqrt{2a\Omega(r^{n+1} - r_h^{n+1}) - R(r) * a^2(n+1) + v_h^2} \qquad \textbf{(3.3)}$$

where

$$R(r) = \ln\left(\frac{r}{r_h}\right)^2 \text{ for } n = 0$$

$$R(r) = \frac{r^{2n} - r_h^{2n}}{n} \text{ for } n \neq 0$$

The velocity at the hub is defined as $v_h \cong \Omega r_h / 0.6$ which is the minimum velocity while maintaining a high aerodynamic efficiency (M. Hurtado et al., 2017).

Therefore, the aim of the design of the velocity profile is to define the hub-to-tip ratio (v), the tip tangential velocity (M_{tan}), and the velocity distribution through the swirl velocity coefficient a and exponent n. To this end, a Multi-objective Genetic algorithm (GA) from the MATLAB toolbox (Chipperfield and Fleming, 1995) has been implemented to investigate the trade-offs between hub-to-tip ratio and tip tangential velocity for a target volumetric flow rate of 1030 CFM. Hence the objective functions to be minimized are the tip tangential velocity (M_{tan}), and the hub-to-tip ratio (v), respectively. Lastly, a constraint function is used to limit the solutions to velocity distributions, i.e. swirl velocity coefficient a and exponent n, that result in the target volumetric flow rate of 1030 CFM. The non-dominating set of feasible solutions (Pareto front) are presented in Figure 8. Here the minimum tip tangential velocity for a range of hub-to-tip ratios that result in the target volumetric flow rate is shown. It can be illustrated here that as the hub-to-tip ratio decreases, the required tip tangential velocity to generate the target volumetric flow rate increases.

The hub-to-tip ratio and corresponding tip tangential velocity selected for the design of the control vortex velocity profiles are 0.405 and 0.105, respectively (green circle). Here, the swirl velocity coefficient and exponent for Equations (3.2) and (3.3) are 4.48 and -0.1922, respectively. The resulting axial and swirl velocities are shown in Figure 9.

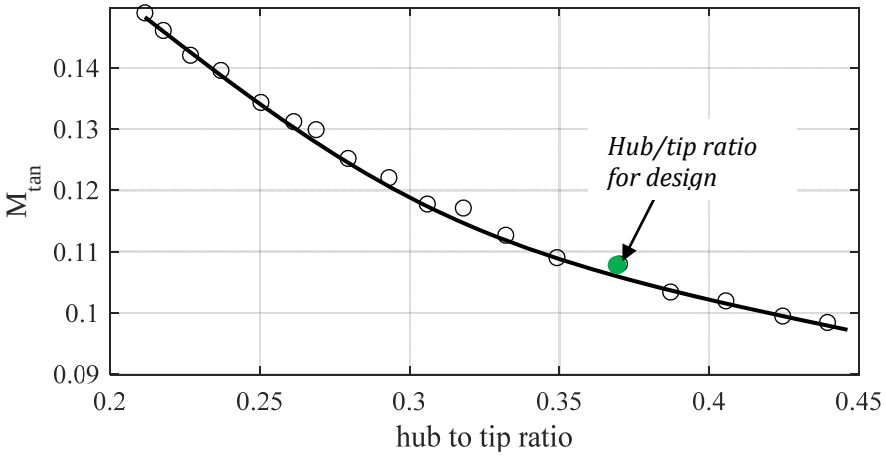

Figure 8: Multi-objective GA Pareto front results.

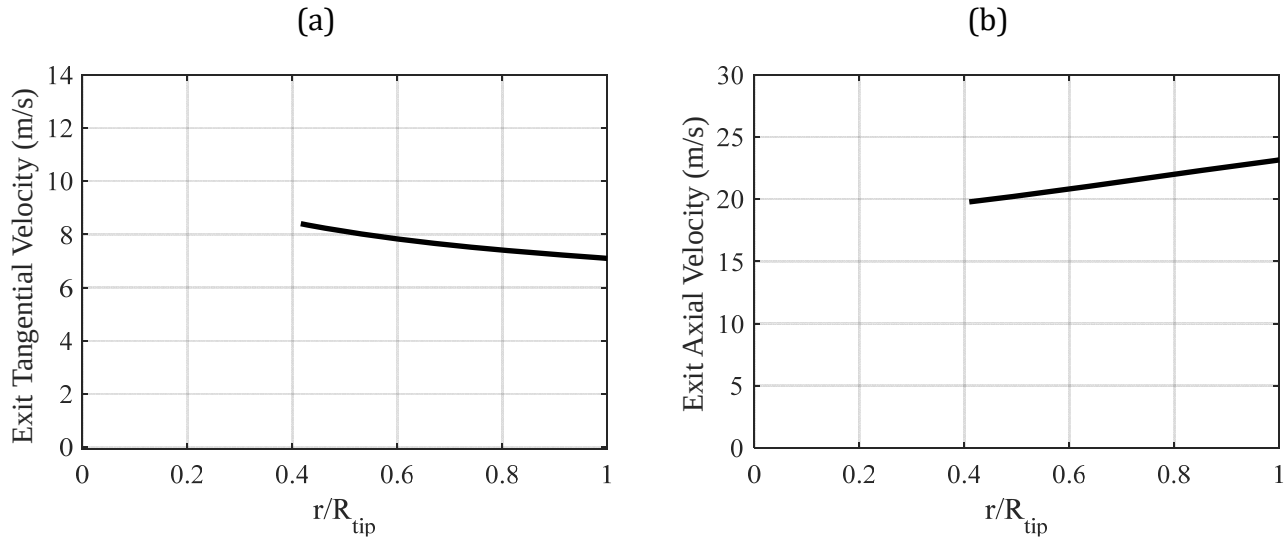

Figure 9: Designed (a) tangential (swirl) and (b) axial velocity distributions.

Fan geometry design

An inverse design method has been implemented to design the blade chord and twist distribution that generate the velocity profiles shown in Figure 9. The constraints imposed on the design of the blades are (a) a chord at the hub less than the hub radius, (b) a chord at the tip greater than 40% of the hub radius, and (c) a twist at the hub less than 85 deg. These constraints were imposed to limit the blade designs to realistic blade geometries that are practical to fabricate. The resulting chord and twist are shown in Figure 10. The 3D blade geometry including the outside shroud is shown in Figure 11. The single fan designed is hereafter referred to as **C**ontrol **V**ortex **T**andem (CVT).

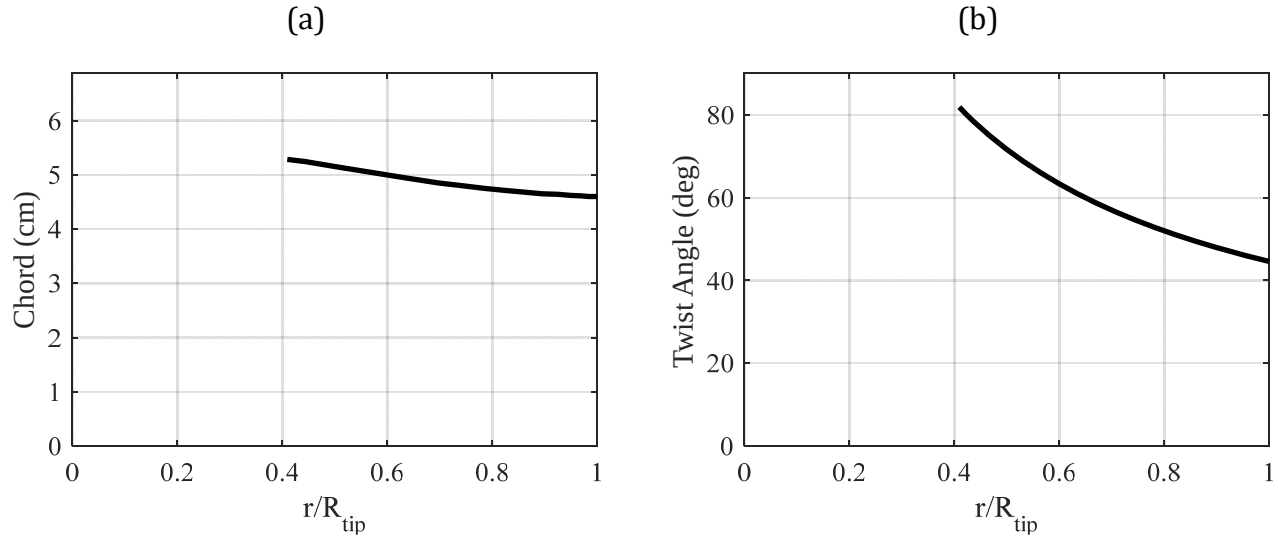

Figure 10: (a) Chord and (b) twist distributions for fan design.

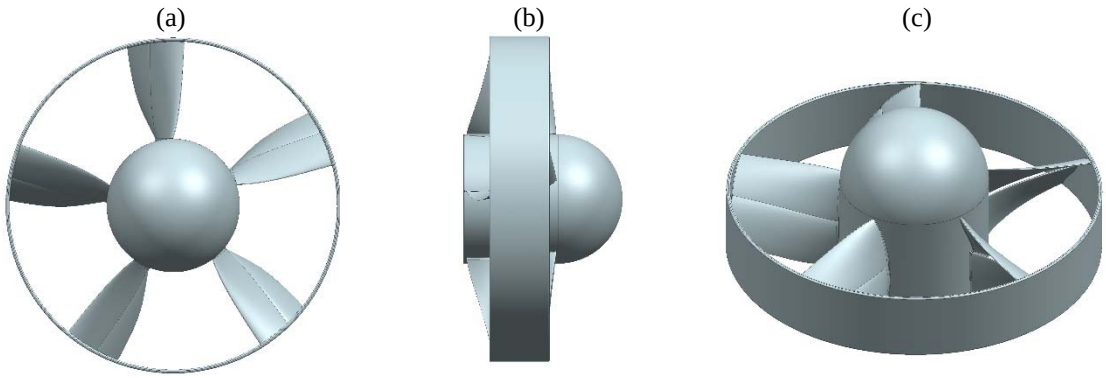

Figure 11: Fan design (a) front view, (b) side view, (d) Isometric view.

It is important to clarify that several fans were designed, fabricated, and tested, including both single and tandem airfoil configurations. However, only the fan selected for the VTFA system is reported in this document.

Motor selection and test rig design

The current trend in the industry is to use BLDC motors to drive the ventilation fans. This is due to their higher efficiency, higher power density, and lower weight relative to other variable speed drives (Yong-Han et al., 2006). However, motor noise arising from the electro-magnetic forces can be a significant source of noise. Therefore, the noise of 5 candidate motors with suitable torque-rpm characteristics have been experimentally tested at Virginia Tech. The aim of this experimental investigation was to select a motor with low noise levels to drive the fans. The 5 motors considered for the test rig are shown in Figure 12 with the corresponding characteristics from the manufacturer datasheets shown in Table 3.

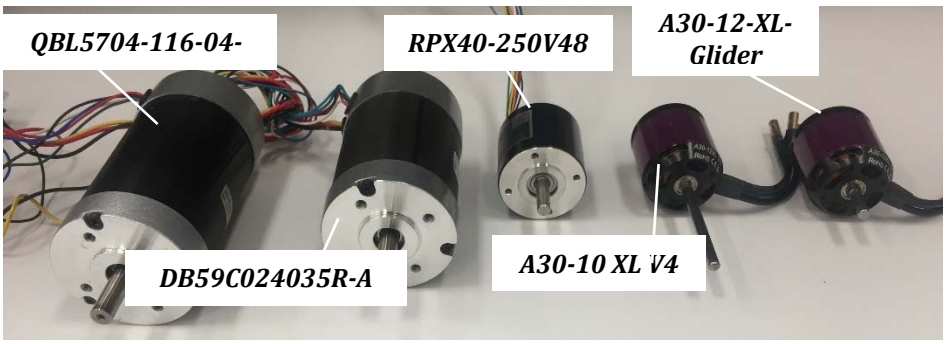

Figure 12: Selected candidate motors.

Table 3: Performance characteristics of the candidate motors.

Motor	Rated torque [n-m]	Rated Speed [rpm]	Power [watts]	Diameter [mm]	Axial length [mm]
DB59C024035R-A	1.79	3500	220	57	93
A30-10 XL V4	0.651	6000	722	43	45
A30-12-XL-Glider	0.5	6100	500	43	48.5
QBL5704-116-04-042	0.42	4000	160	57	116
RPX40-250V48	0.25	4075	140	41	40

The candidate motors were tested unloaded in the reverberation chamber at Virginia Tech using the experimental set up shown in Figure 13. The volume of the reverberation chamber is 46.67m^3. The measurements were performed using 8 microphones placed away from the source and the hard surfaces (in the reverberant field) randomly placed in the room. The sound power level is computed as:

$$Lw(f) = L_{spl,avg}(f) + 10\log_{10}(V) - 10\log_{10}(T_{60}(f)) - 13.9 \quad \textbf{(3.4)}$$

where $L_{spl,avg}$ is the average sound pressure level measured by the microphones, V is the volume of the reverberation chamber, and T_{60} is the reverberation time. The speed of the BLDC was measured using the optical sensor shown in Figure 13. The measured 1/3rd octave band sound power spectra for the 5 candidate motors (unloaded) is presented in Figure 14 and Figure 15 at 3000 and 4000 rpm, respectively. It is clear form Figure 14 and Figure 15 that the DB59 and QBL5704 motors are the better options to drive the fan since they are significantly quieter than the other 3 motors. However, the size of the DB59 motor is significantly smaller than the QBL5704 motor as shown in Figure 12. Therefore, due to the compactness, power, design speed, and noise level the DB59 motor has been selected to drive the fan design (green results in Figure 14 and Figure 15). The motor spectrum for the DB59 motor at different speeds is presented in Figure 16. As illustrated here the sound power level for the DB59 motor at full speed (4500 rpm) is 54.4 dBA. To this end, the DB59 motor was chosen to drive the fan design.

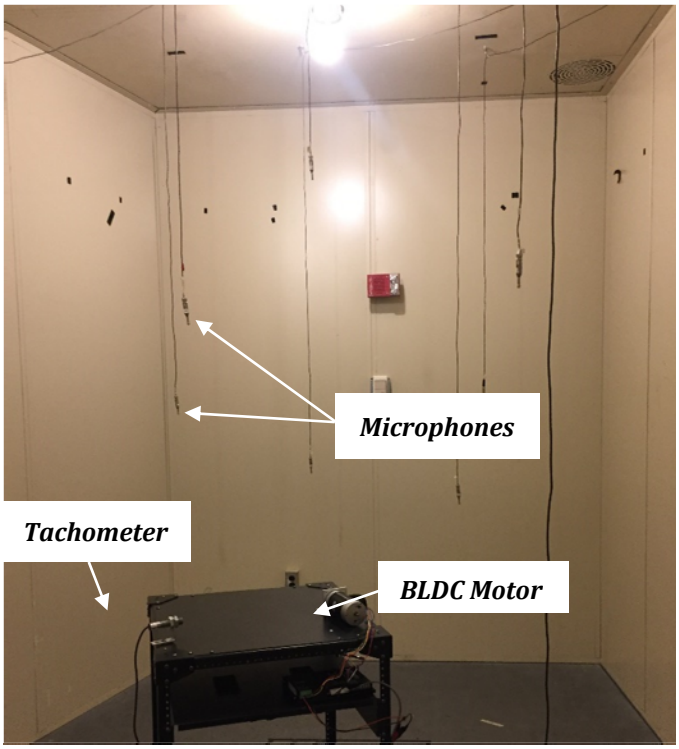

Figure 13: Test set up in the reverberation chamber.

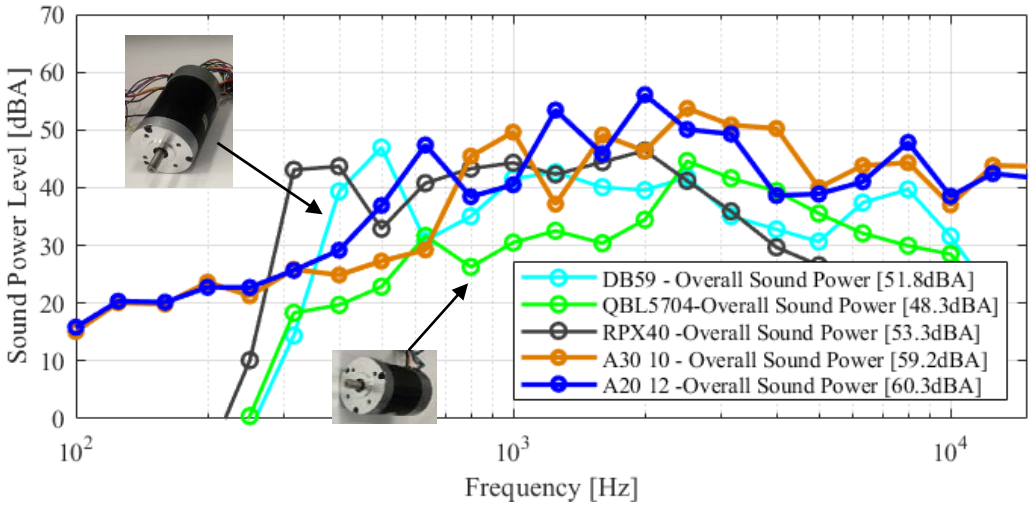

Figure 14: Sound power level spectrum for candidate motors at 3000 rpm.

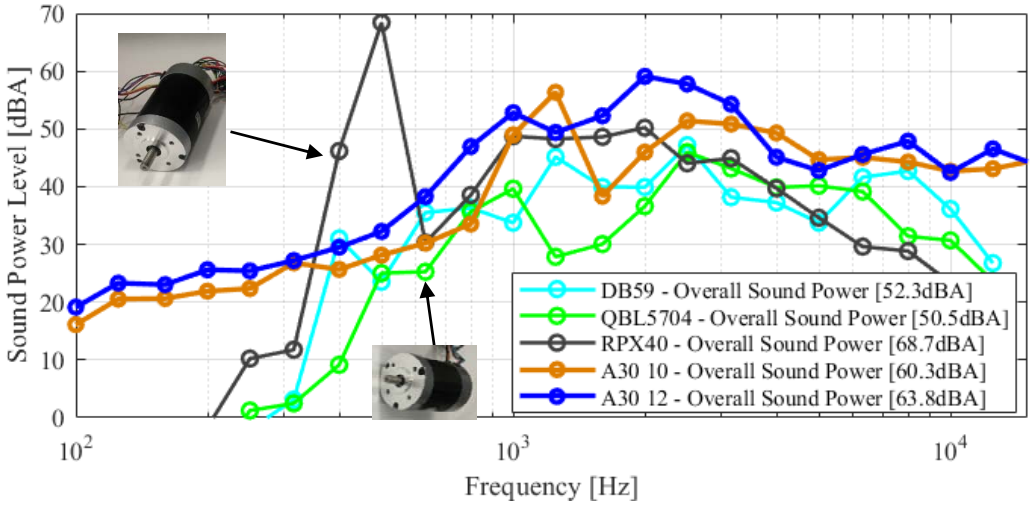

Figure 15: Sound power level spectrum for candidate motors at 4000 rpm.

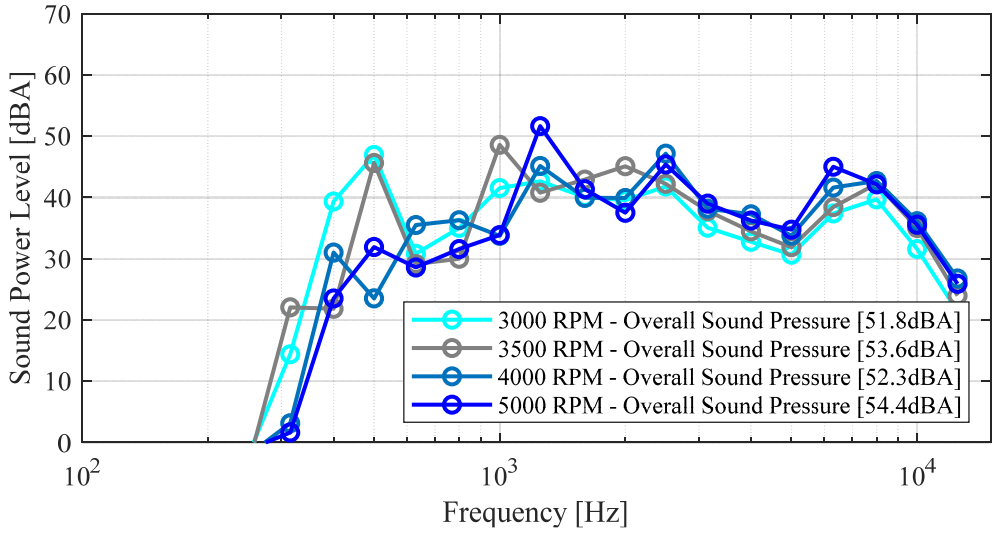

Figure 16: Sound power level spectrum for the selected motor at different speeds.

The DB59 BLDC motor was integrated into the design of a test rig to test the fan. The motor is coupled to the fan using a motor shaft collar and a mounting plate as shown in Figure 17a. The motor is supported by a motor clamp and a swept strut downstream of the fan. An aerodynamic motor sleeve is added to eliminate the cavity (or backward and forward) steps between the fan and the motor and eliminate the potential for parasitic noise. The fan is then enclosed with an inlet and outlet duct. Additionally, a rotating shroud is added to the fan to eliminate the leakage flow from generating tip gap noise as shown in Figure 17b and Figure 17c. The rotating shroud also increases the structural strength of the blades and potential damage of the brittle 3D printed material.

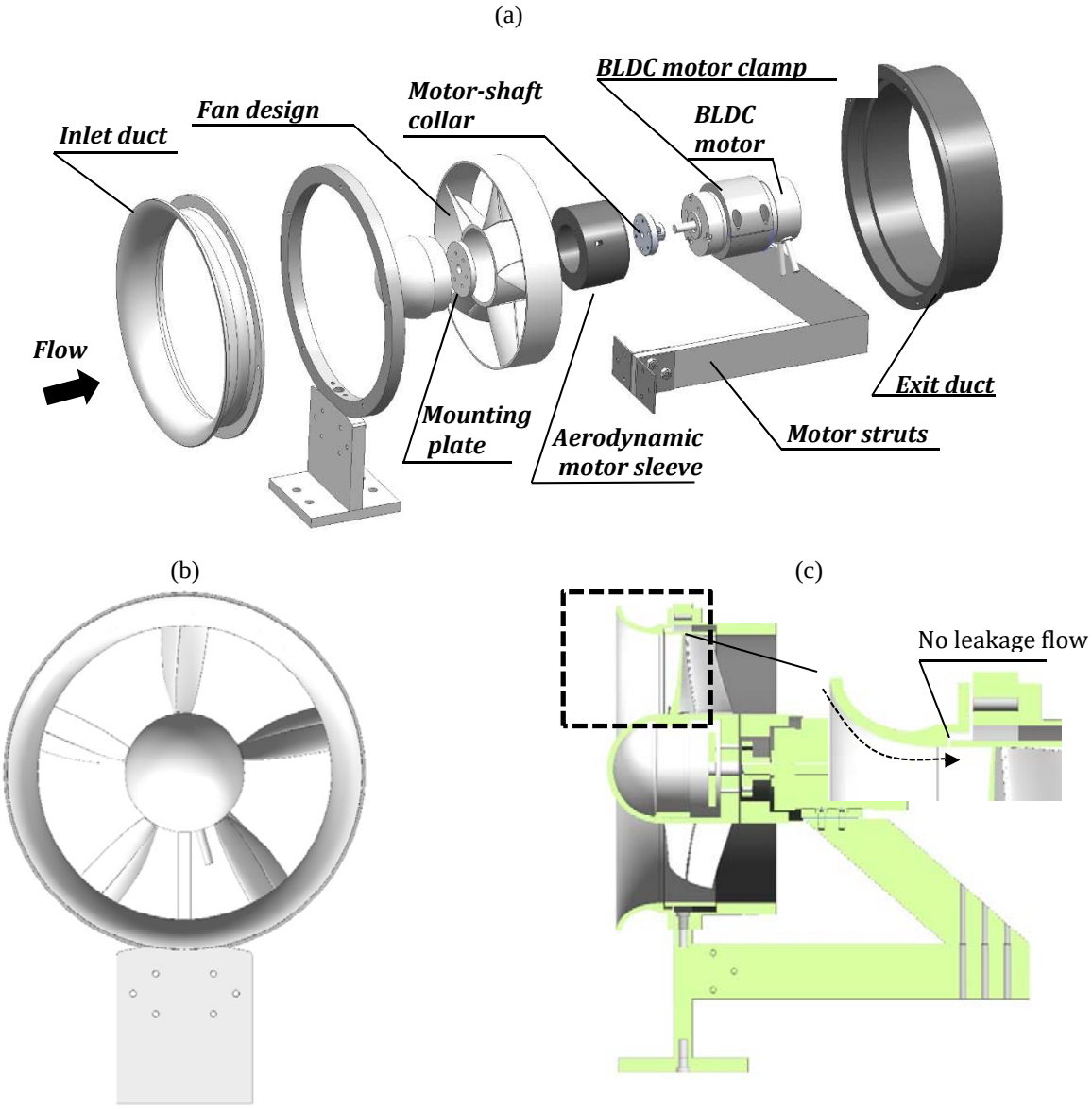

Figure 17: (a) Exploded, (b) side and (c) cross section views of the fan test rig.

Experimental Testing

Instrumentation

The designed fan was 3D printed and tested inside the anechoic chamber (cutoff frequency of 100 Hz) at Virginia Tech. The main noise instrumentation was a 2.8 m diameter far-field arc array as shown in Figure 18. The far field arc is composed of 19 microphones evenly distributed along its circumference, i.e. from 0 to 180 degrees. The center of the arc array has been placed at the center of the fan. The fans have been 3D printed using an opaque white SLA plastic that behaves similarly to a polypropylene/ABS mix. The tolerances in the X/Y/Z dimension are ±0.001"/in. (0.001mm/mm).

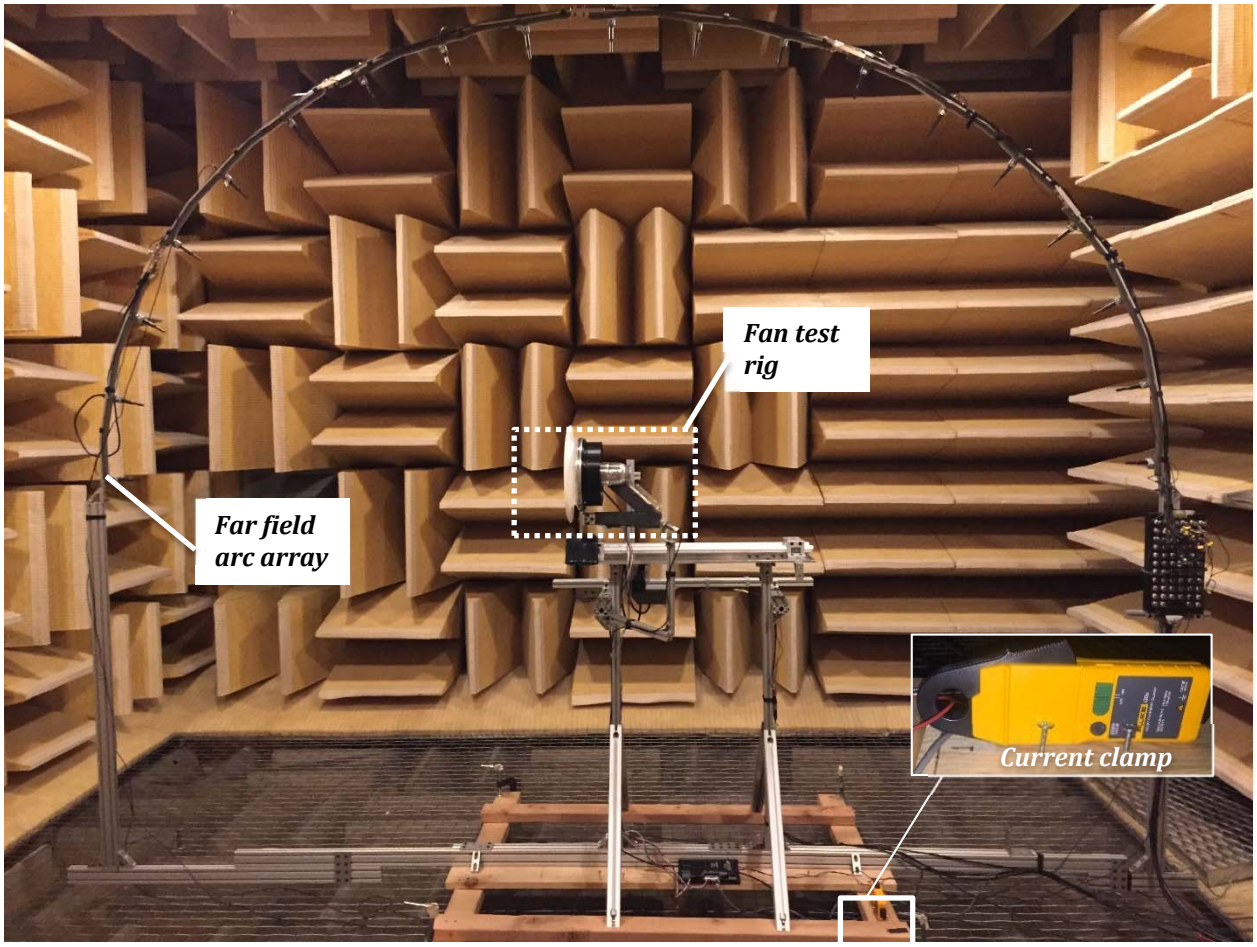

Figure 18: Noise measurements using the far field arc array.

The flow test apparatus consists of a Haydon LRS linear actuator, a Dwyer Series 160 Stainless Steel Pitot-static tube, and a Setra Systems 264 differential pressure transducer as shown in Figure 19. The Pitot-static tube has a calibration factor of 1, i.e. no calibration needed, with an accuracy of +/- 2% (Dwyer, 2016). The Pitot-static tube is mounted on the linear actuator which it is used to traverse the Pitot-static tube across the duct. The flow velocity profile is used to compute the volumetric flow rate. The angular velocity of the fan was recorded using the optical sensor shown in Figure 20. The optical sensor used for this measurement is model ROS-P-25 by Monarch

Instrument. The optical sensor has been mounted as shown in Figure 19 and emits a light beam to the rotating retro-reflective tape on the fan hub. The optical sensor then generates a constant ~5 volts signal (TTL signal). The tachometer uses the optical sensor pulse signal to display the rotational speed in rpm as shown in Figure 20. The motor torque was estimated by measuring the motor current and multiplying it by the motor torque constant. The motor current was measured using an i30s current clamp meter. The current clamp meter measures the motor current with an accuracy of ± 1 % of reading ± 2 mA by clamping the jaws around the motor drive power cable as shown in Figure 21. The fan torque is computed as the difference between the fan/motor configuration torque and the motor only toque. The fan mechanical power is computed as the product of the fan torque and the fan speed.

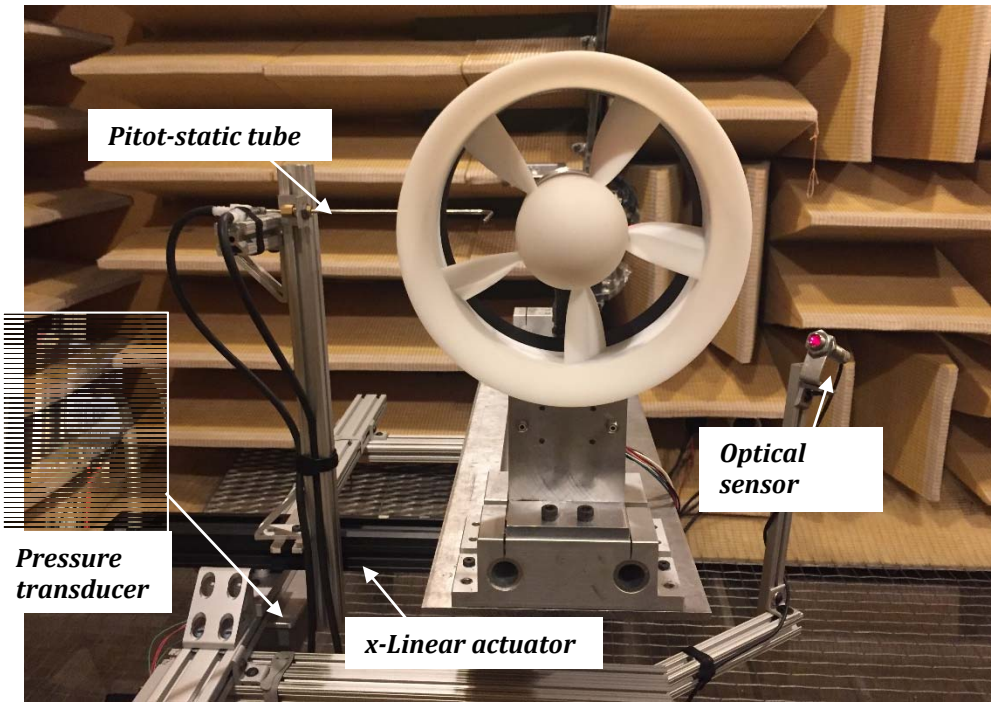

Figure 19: Fan test rig front view.

Figure 20: (a) Optical sensor and (b) tachometer used to monitor fan speed.

Figure 21: i30s current sensor.

Experimental Results

The measured mechanical power is compared to the predicted mechanical power in Figure 22. As illustrated here, the measurements agree very well with the predictions. Furthermore, it can be shows that the repeatability is also very good up to the design speed of 3500 rpm.

The axial velocity profile is compared to predictions for two different speed in Figure 23. Here it can be observed again that the agreement is excellent. It is important to note that a cross section of the fan is shown in the figures with an estimate of the boundary layer thickness indicated in dashed blue lines.

Consequently, the design process implementing multi-element airfoils has been validated. The excellent results here also indicate that the predictions of the multi-element polars using MSES/MSIS is very accurate.

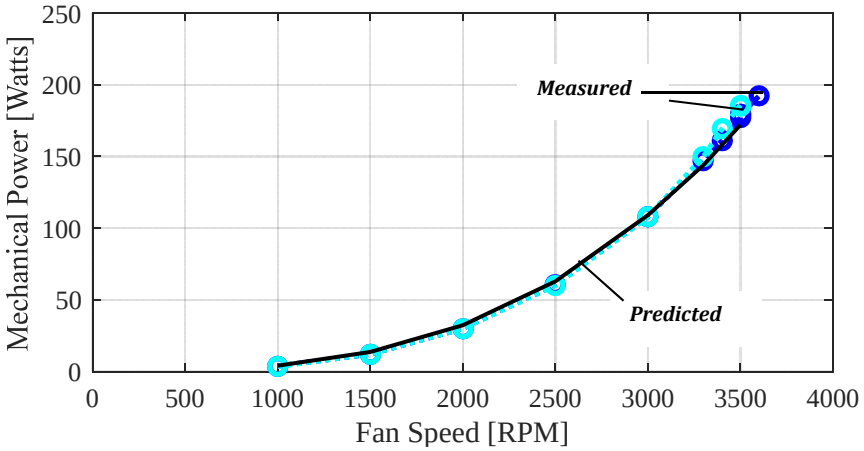

Figure 22: Measured and predicted mechanical power vs fan speed.

(a)

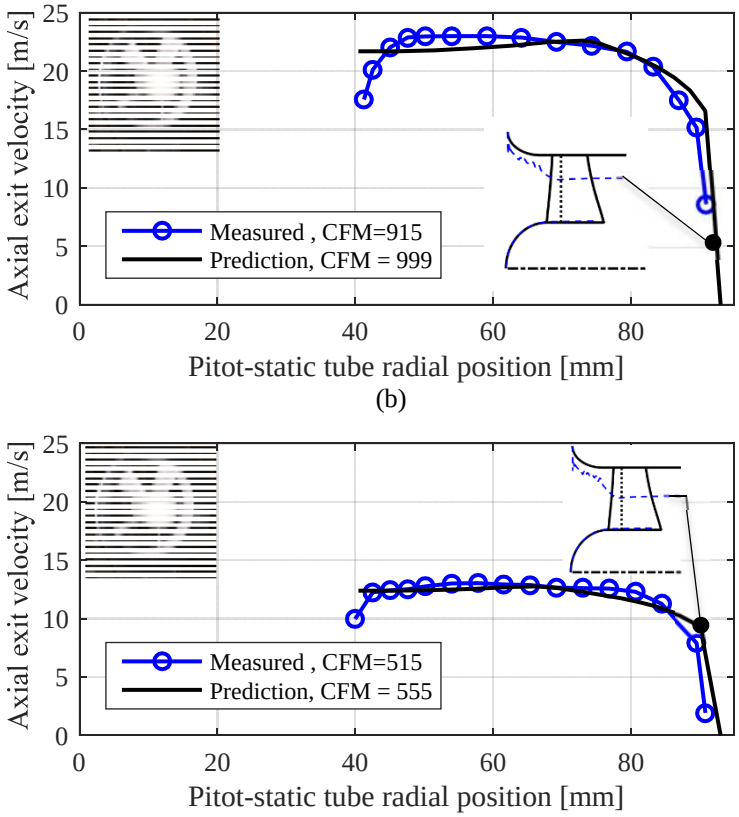

Figure 23: Fan velocity profiles at (a) 3500 rpm (b) 2000 rpm.

3.2 Phase 2: VTFA unit design

This section presents the design and experimental investigation of the VTFA unit. To this end, the best fan designed and validated in phase 1 is incorporated into an array of 7 fans, all driven by individual motors (DB59 motor).

VTFA Unit Fabrication

Figure 24 shows a CAD drawing of the VTFA unit. The seven fans are mounted to the motors using the same mechanism used in the design of the single fan test rig, i.e. same components shown in Figure 17a. The fan-motor assemblies are then mounted to an aluminum baseplate fixed inside of a cylindrical duct. The VTFA incorporates an inlet bell-mouth to clean the inflow and minimize inflow turbulence due to the sharp leading edge of the duct. Additionally, all seven fans have individual bell-mouths (labeled as inlet channel) with the same geometry used when testing the single fan. The inside diameter of the VTFA unit is 0.68 m (27 inches) while the length is 0.4 m (16 inches).

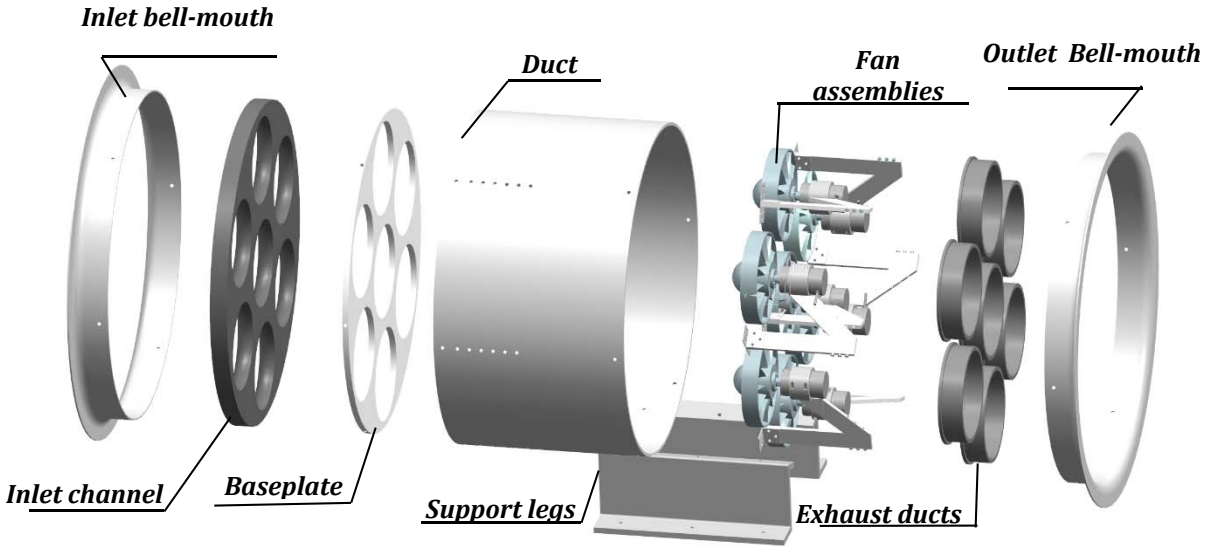

Figure 24: Exploded view of VTFA unit (duct diameter 0.68 m).

The VTFA unit has been fabricated through traditional machining and 3D printed parts. To this end, the inlet channel and exhaust ducts were 3D printed using FDM (Fused Deposition Modeling) with a standard ABS material. The maximum layer height is 200 microns. The fans were 3D printed using an opaque white SLA. A multi-axis DMC-4070 controller is used to drive all of the fans. The controller is powered by an AC-DC Power Supply. Figure 25 shows a front view of the VTFA unit and components. As illustrated here, the tip gap is eliminated using the fan's shrouds, similarly to the single fan test rig. Additionally, the flow blockage is minimized using the same struts configuration as for the single fan test rig. The rear view of the VTFA unit is shown in Figure 26. As illustrated here, obstructions downstream of the fans are minimized, i.e. motor power cables are taped downstream of the fan struts. Figure 26 also shows that the soft foam has been added to the motor struts as they help reduce fluid-strut interaction noise. The motor encoder shown in Figure 26 is used to drive the motors using the DCM-4070 controller at a given speed.

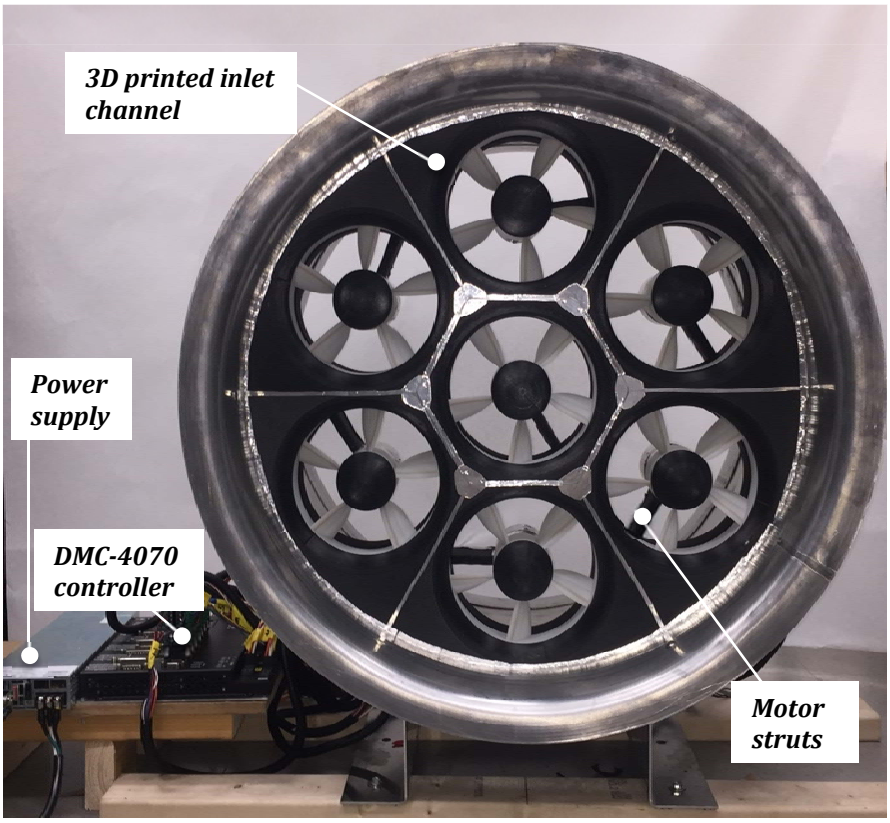

Figure 25: VTFA unit picture view from the front.

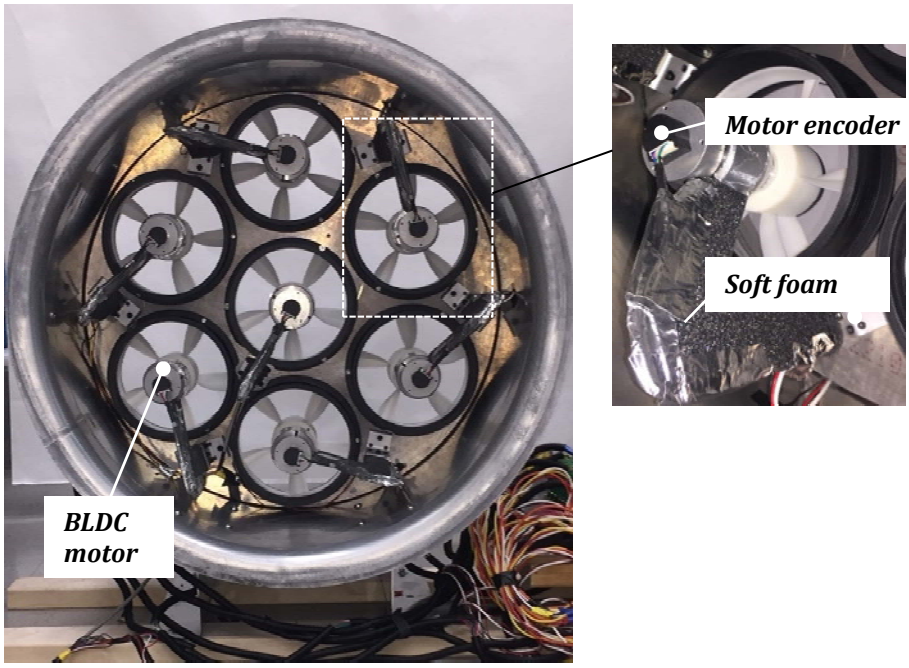

Figure 26: VTFA pictures (a) rear and (b) top views.

VTFA Unit Flow Measurements

Volumetric flow rate have been carried out to characterize the performance of the VTFA unit relative to commercial ventilation fans. The same measurements were performed on the baseline Cincinnati fan in the previous project (award AFC215-21 -(Burdisso et al., 2017). Thus, the results can be compared directly. To this end, an anemometer has been used to measure the flow at 57 locations on the exit plane of the VTFA unit as shown in Figure 27. The measurements were made at azimuth angles of 0, 45, 90, 135, 180, 225, 270, 315 degrees and at 7 radial positions ($r/R = 0.15, 0.3, 0.45, 0.6, 0.75,$ and 0.95). The speed of the fans was controlled using the multi-axis DMC-4070 controller. The fans were assigned identification numbers as shown in Figure 27.

The flow measurements have been interpolated to generate axial flow velocity maps. Figure 28 shows the flow map at a fan speed of 3064 rpm with motors 1 and 4 turned off. The volumetric flow rate is 6626 CFM. The color contour plot clearly shows very low flow velocities from these two fans, as expected. Figure 29 presents the measured volumetric flow rate as a function of fan rpm for the VTFA unit. For reference, the results for the single fan tested in phase 1 is also plotted. It is interesting to note that the CFM produced by the VTFA unit is about 15% higher that the CFM estimated from adding the contribution from 7 individual fans. For example, at a fan speed of 3000 rpm the single fan generates 768 CFM. Thus, assuming 7 individual fans the total CFM would be 769x7 = 5383 CFM. However, testing of the VTFA unit shows 6311 CFM at 2900 rpm. The dashed line in the figure is the estimate CFM for the VTFA unit based on the single fan CFM data. The increase in volumetric flow rate for the VTFA is probably due to two factors: a) the addition of the unit inlet bell-mouth and b) the large duct aligning the streamlines more in the axial direction as the flow travels downstream. A computational fluid dynamic (CFD) analysis would be required to fully investigate this benefit in CFM but it is outside the scope of the project.

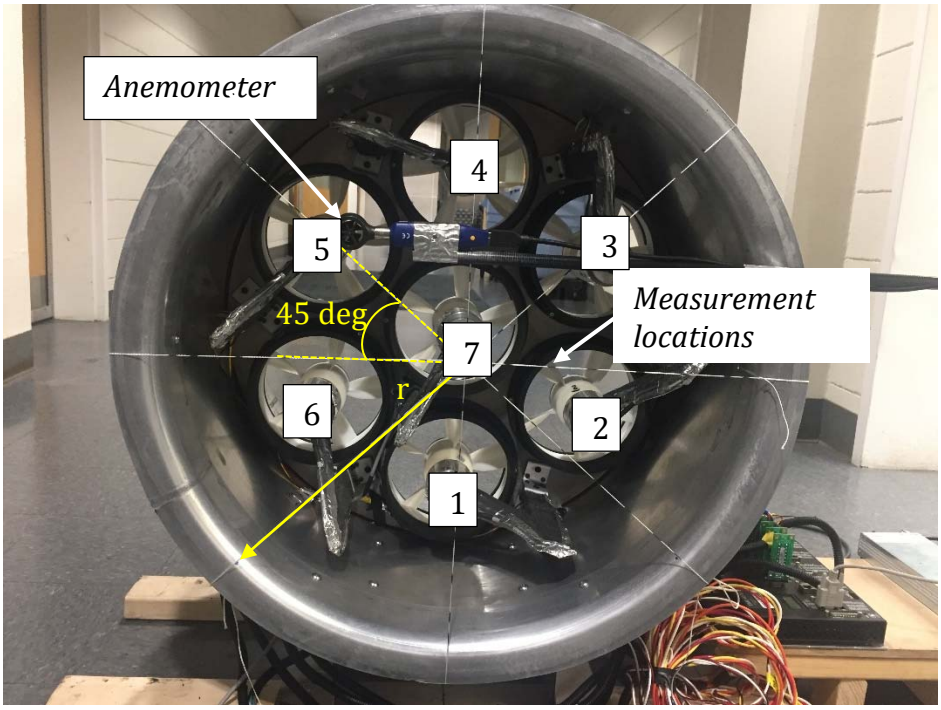

Figure 27: Flow measurement locations and fan identification number (view from the back).

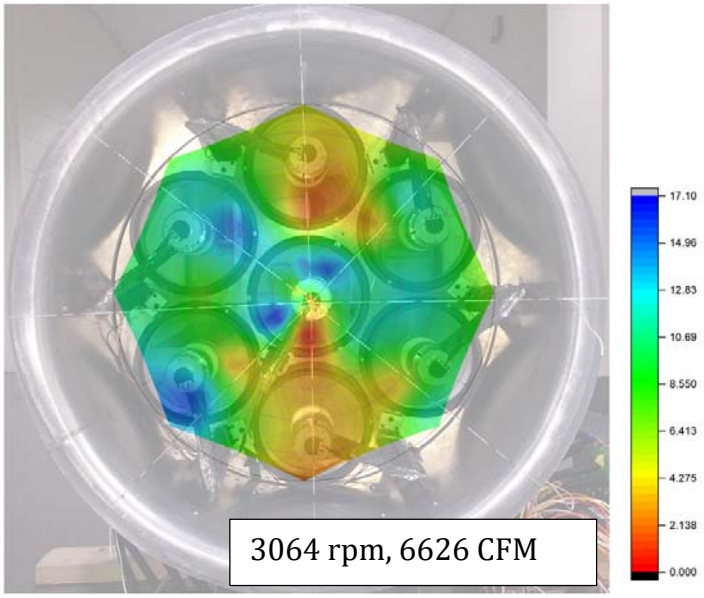

Figure 28: Flow measurements at 3000 rpm with motors 1 and 4 off (view from the back).

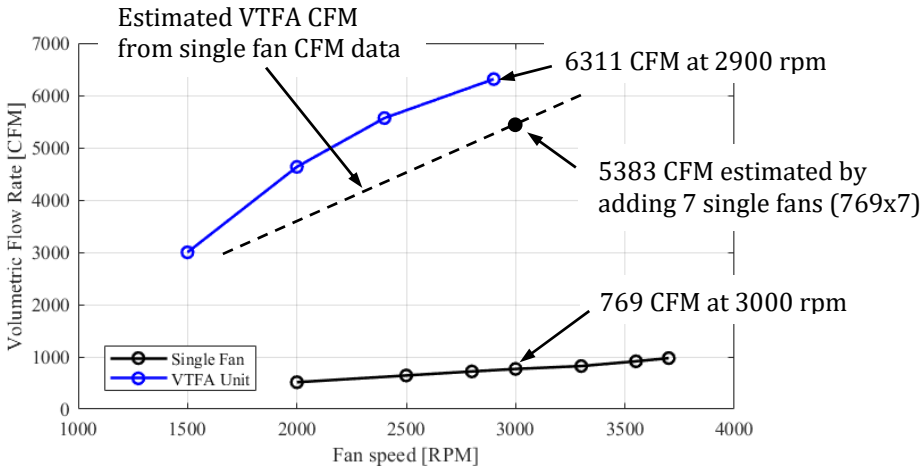

Figure 29: Measured volumetric flow rate as a function of fan speed. Dashed line is the estimated VTFA CFM based on adding the contribution of 7 single fans.

VTFA Unit Noise Measurements

Noise measurements of the VTFA unit were performed outdoors due to the large size of the unit. The noise measurement approach was the same as for the baseline Cincinnati fan so results can be compared directly. Figure 30 shows the fan unit under test. To reduce reflections a 3.5 feet tall and 8.5 ft wide wall of acoustic wedges was built on both sides of the fan. The measurements were made with an arc array of 19 microphones evenly distributed along its circumference.

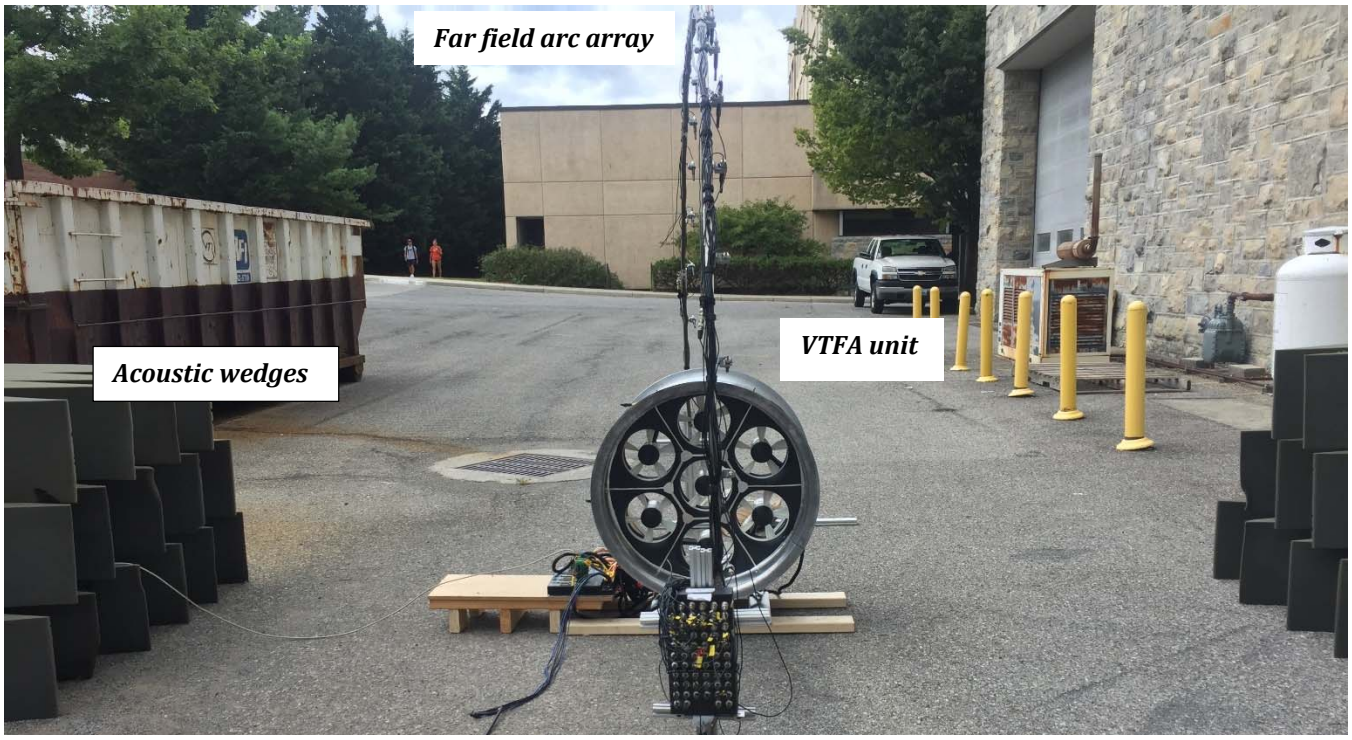

Figure 30: Noise measurements experimental setup (flow into the page).

Figure 31 shows the narrowband sound power spectrum measured at 2500 rpm (red line). The background noise was also measured and plotted (blue line). The signal to noise ratio is ≥10 dB at 400 Hz and higher frequencies. Thus, there is no need for background correction in this frequency range. The overall sound power level for the VTFA unit is 84.6 dBA. The spectrum reveals a few interesting and important features. Firstly, the spectral shape is a very smooth broadband component with a strong roll off starting at 4000 Hz. Secondly, a hay-stack at ~1000 Hz is observed for the VTFA unit that was not present in the test of the isolated fan in phase 1 (black line) fan. This hay-stack mechanical noise is due to vibration induced by the fans. It is believed that the struts supporting the motor-fan go into resonant motion at ~ 1000 Hz driven most likely by the unbalance of the motor-fans. The vibration can be significant and resulting in some of the fans touching the duct exacerbating the problem. Thirdly, both the VTFA unit and the background spectra show highest broadband levels below 400 Hz (yellow zone). This effect is very likely due to the windy conditions the day of the test (steady wind of 8 mph with some gusts) and the turbulence ingested due to the fan been so close to the ground (see later results in Figure 32 for more details). The ingested turbulence interacting with the fans results in the high VTFA unit noise levels in the low frequency range.

To gain more insight, an estimated of the VTFA unit noise was performed by taking the spectrum from the single fan noise measurements in the anechoic chamber and assuming that all 7 fans produce the same noise incoherently. That is the VTFA unit noise can be estimated as

$$L_{w,VTFA}(f) = L_{w,\text{single fan}}(f) + 10\log_{10}(7) \qquad \textbf{(3.5)}$$

where $L_{w,\text{single fan}}(f)$ is the sound power spectrum of a single fan (measured at 2500 rpm in phase 1), and 7 is the number of fans resulting $10\log_{10}(7) = 8.5dB$. The estimated noise for the VTFA unit , $L_{w,VTFA}(f)$, is shown in Figure 31 (black line) with an overall power level of 79.5 dBA (or 18.8 dB reduction relative to Cincinnati fan). The estimated (black line) and measured (red line) VTFA noise matches very well at ≥2000 Hz. Since the single fan noise spectrum was determined in the anechoic chamber, it is not affected by turbulence. Thus, the measured VTFA noise (red line) in the low frequency range is clearly due to turbulence (caused by the windy conditions and close proximity to the ground) interacting with the fans. Thus, the difference between the overall noise level 84.6 dBA (measured) and 79.5 dBA (estimated) is due to turbulence ingestion (noise at low frequency).

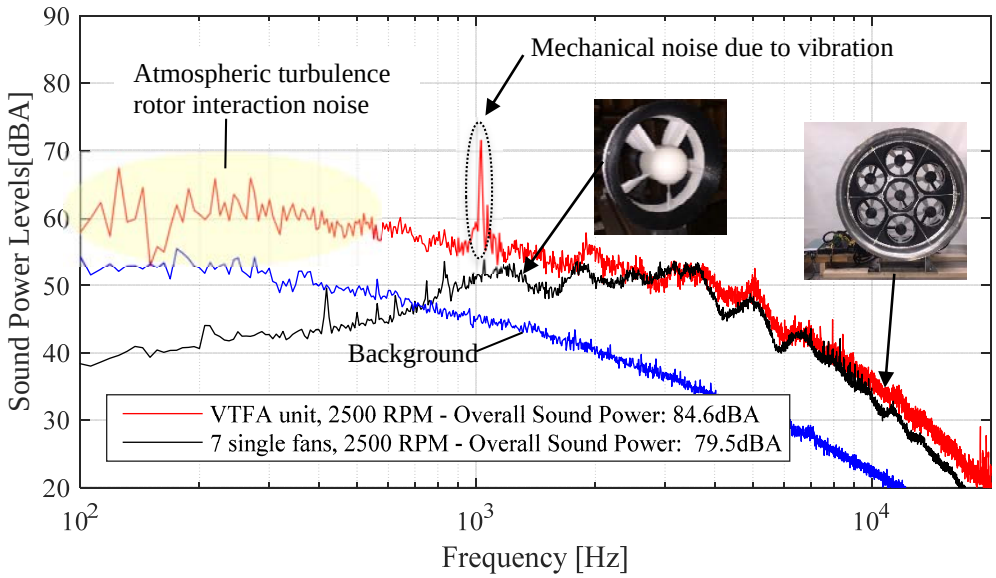

Figure 31: VTFA unit narrowband sound power spectrum measured and estimated: a) red line is measured VTFA unit, b) black line is estimated from single fan test in anechoic chamber and increased by 8.5 dB to account for 7 uncorrelated fans, an c) blue line is background noise.

The VTFA unit noise is compared to the Cincinnati fan in Figure 32. In this figure, the measured narrowband acoustic power spectrum for the VTFA unit at two configurations and for the baseline Cincinnati fan are shown. In Figure 32a, VTFA unit was operated at 2800 rpm with all fans on. In Figure 32b, the VTFA unit was operated at 3100 rpm but with fans 1 and 4 turned off. The results in both cases show that the VTFA unit produces significantly less noise over the key frequency range of interest (100 to 4000 Hz). The noise from the motor is visible in the tones at high frequency (7 to 10 kHz) in Figure 32b. Motor noise has nearly insignificant contribution to the overall noise level. The results also show that the VTFA unit do not shows any blade passage frequency (BPF) tones typical of fans. For example, the Cincinnati fan shows tones at the BPF (~ 180 Hz) and its harmonics. The reason that the VTFA doesn't have the BPF and harmonic tones is that the individual fans were operated all at slightly different fan speeds (approximately +/- 10 rpm) thus eliminating the constructive interference between the fans at the BPF tones, e.g. acoustic energy was scattered out over a range of frequencies rather than a single one.

It is also interesting to note that the VTFA unit is significantly quieter for the case in Figure 32b (fans 1 and 4 are off while the other fans operate at 3100 rpm) as compared to the case in Figure 32a (all fans operating at 2800 rpm). However, in both cases the volumetric flow rate is nearly the same, e.g. 6311 vs 6626 CFM. The decreased in noise for the case in Figure 32b (fans 1 and 4 off) is likely due to fan 1 ingesting significant amount of flow distortion and turbulence because of proximity to the ground and hence it generates the most noise.

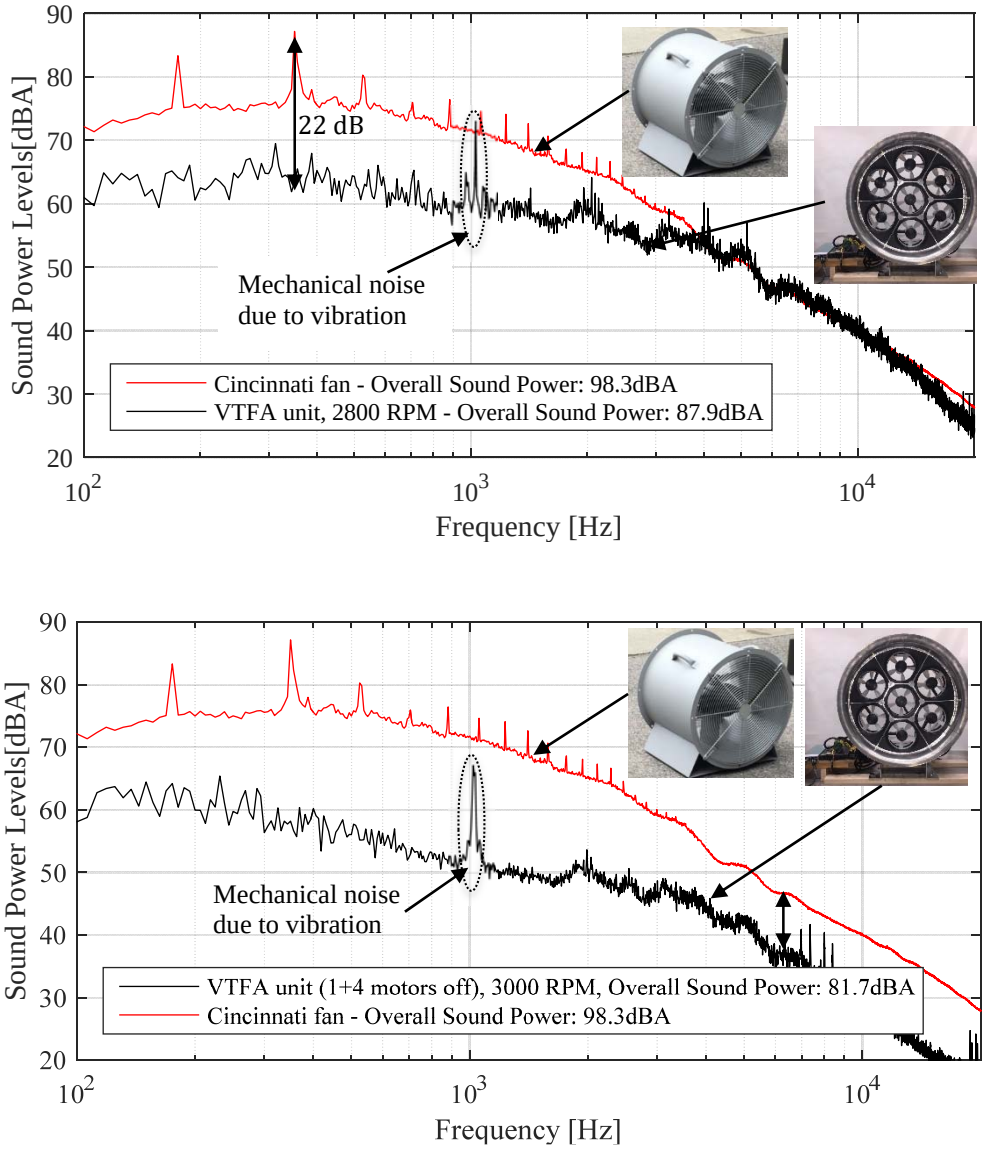

Figure 32: Narrowband power spectrum for (a) VTFA unit at 2800 rpm with all fans on and (b) VTFA unit at 3064 rpm with fans 1 and 4 off. In both cases Cincinnati fan operates at 1750 rpm.

To summarize the noise results in a single plot, Figure 33 shows the overall sound power level for the VTFA unit as a function of fan rpm with all 7 motors operating (blue line). For reference, the case of 5 motors operating at 3064 rpm (motors 1 and 4 are off) in Figure 32b is also included as a solid black circle. The Cincinnati fan noise is indicated by the solid red circle at 98.3 dBA. The results

for the single fan as a function of rpm measured in the anechoic chamber is also included (black line). The noise produced by 7 of these fans (incoherent addition) results in the single fan noise results to be shifted up by 8.5 dB (dashed black line). This line represents the quietest possible configuration with all 7 fans operating, e.g. unaffected by atmospheric turbulence and flow distortion from ground.

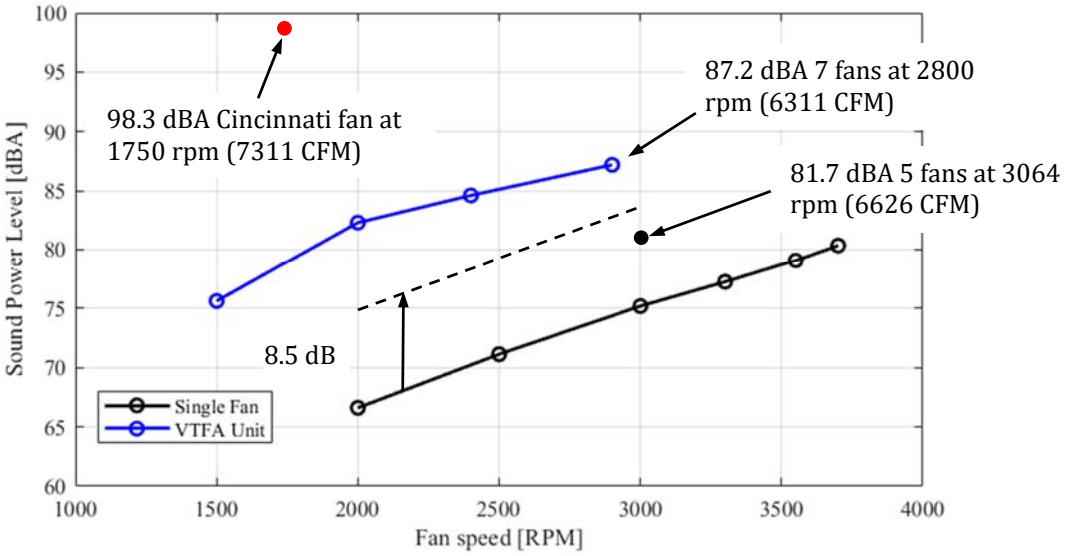

Figure 33: Overall sound power level as function of fan rpm.

4. Research Findings and Accomplishments:

The aim of the proposed research was to build upon the tools and findings of award number AFC215-21 to design and test a quiet ventilation fan array unit to experimentally demonstrate significant noise reduction while maintaining or increasing the volumetric flow rate (CFM) as compared to existing commercial fans. In particular, the Cincinnati fan model 24631 was used as the baseline case for detailed comparisons. The specific aims were: i) to implement a fan array concept where a large single fan was replaced by an array of smaller fans; ii) to implement a multi-element blade to further allow the reduction of the fan speed and noise; and iii) to implement a quiet motor to drive the fans to eliminate the motor as a noise source.

The fan array concept was successfully developed, fabricated and tested. It did meet the design goals of quiet operation, compact size, and with very good aerodynamic performance. The ambitious noise reduction goal of 25 dB reduction relative to the Cincinnati fan was not achieved (best reduction was 16.6 dB). However, there are positive research findings from implementing the fan array concept. They are:

a. The flow rate for the fan array was ~15% higher than combining the flow rate from the individual fans. This implies that the performance of the fans is not adversely compromised due to their close proximity. It is likely that the presence of the large duct enclosing the fans provides this benefit.
b. The dominant noise source in the fan array is the interaction of the rotor with atmospheric turbulence (due to outdoor testing) and flow distortion due proximity to the ground. Since ventilation fans are typically operated indoors, the ambient turbulence should not be a serious problem. Moving the fan further off the ground should also reduce the effect of ground flow distortion.
c. The operation of the fans in the array at slightly different speeds completely eliminated the presence of tones at the blade passage frequency (BPF) and harmonics typical of single fan units. This advantage of the fan array system was demonstrated experimentally.

The implementation of multi-element blades is likely the most important accomplishment in this project. It is important to note that there are no reported results of low speed fans using multi-element airfoils in the open literature. Thus, this work has demonstrated for the first time the potential of this innovation. Specific accomplishments related to the multi-element technology are:

a. It was demonstrated that an optimized 2-element blade yields a significant increase in lift while moderately increasing the drag losses. This allowed to reduce the fan tip speed to a very low 0.1 tip Mach without compromising aerodynamic efficiency.
b. For the design of fans, it is critical to compute the blade polars accurately. The excellent agreement between predicted and measured aerodynamic results (flow distribution and torque) demonstrated the accuracy of the MSES/MSIS code used to predict the polars for multi-element airfoils. There is again no relevant published experimental data for the multi-element polars to rely on as for the case of single element airfoils.

Finally, it was demonstrated in the fabricated fan array system that the motor noise can be eliminated as a dominant source. This was accomplished by careful testing and selection of candidate quiet BLDC motors.

5. Publication Record and Dissemination Efforts:

The presentations and publications resulting from this research are listed below:

- **Conference presentation:** Hurtado, M., and Burdisso, R. (2018). Low speed control vortex axial fan design for minimum noise, INTER-NOISE and NOISE-CON Congress and Conference, Chicago, IL, August 26-29.

- **Conference presentation**: Hurtado, M., and Burdisso, R. (2019). Axial Fan Design Using Multi-Element Airfoils to Minimize Noise, INTER-NOISE and NOISE-CON Congress and Conference, Madrid, Spain, June 16-19.

- Hurtado, M., and Burdisso, R. (2019). Low Speed Ventilation Fan Design Procedure for Minimum Noise. Noise Control Engineering Journal (in preparation).

- Hurtado, M., and Burdisso, R. (2020). Design of Axial Fan Incorporating Multi-Element Airfoils to Minimize Noise. Journal of Sound and Vibration (in preparation).

All the tasks originally planned in the proposal have been completed. The project has been documented in its entirety in this final report.

It is important to mention that the fan design methods, airfoil and fan modeling tools and results, testing procedures and experimental data developed under the two Alpha Foundation projects are extensive documented in full details in Mr. Hurtado's Dissertation ("Low speed ventilation fan design for minimum noise"). This document will be available to the public at the Virginia Tech electronic archive systems for theses and dissertation (ETD) upon Mr. Hurtado fulfilling the doctoral requirements (completion date November 2019).

6. Conclusions and Impact Assessment:

As part of this project, a new optimized design methodology for low speed ventilation fans was developed and validated. Unlike previous design methods, this new approach accounts for both aerodynamics and acoustics performance. The implementation of multi-element airfoils was also investigated. This is the first time such technology is used in low speed fans as an enabling technology to reduce the fan speed while maintaining aerodynamic efficiency. The concept of fan-array unit was also explored and a prototype system fabricated and tested. The best result showed a noise reduction of 16.6 dB relative to the selected baseline commercial fan. The testing also revealed that a significant noise source was the turbulence (ambient and from ground) ingested by the fan. This turbulence noise source was uncovered from the observation that operating 5 fans resulted in a reduction of 5.5 dB which it was much greater that the 1.4 dB noise reduction expected by turning off 2 out of the 7 fans. The turbulence can be mitigated using screens and elevating the fan from the ground. Without this turbulence, the expected noise reduction would have been conservatively 18.8 dB. Another important observation from the testing of the fan-array system was the complete elimination of the tonal noise from the periodic passage of the blades, e.g. blade passage frequency (BPF) tone and harmonics. This was accomplished by operating the 7 fans all at slightly different speeds. Though the tones do not contribute significantly to the overall sound pressure levels, their elimination improves the "acoustic quality" of the fan unit, e.g. removing of

annoying tones. In a single fan design, the BPF tones would be present as is the case for the baseline fan.

The most important conclusion from the two projects is that it is completely feasible to design quiet, compact and efficient ventilation fans. In fact, it can be virtually guaranteed that fans with the innovations investigated here will provide at a minimum 15 dB quieter operation than the "typical" commercial fan. This noise reduction will clearly improve the health and safety of workers, not only in the mining field, but in all industries that regularly uses ventilation fans. Though there is a likely increase to the fan cost for some of these technologies (e.g. multi-element airfoils), this additional cost should be considered in lieu of the likely reduction in health care cost and improved productivity associated to having a better working environment.

7. Recommendations for Future Work:

The following are recommendations for future work:

a) As indicated before, the multi-element airfoil innovation is the most important accomplishment from the work here. In some applications, fans are used in combination with exit guide vanes (EGVs) such as large mine ventilation fans (> 8 feet diameter) or high speed fans (scrubber fan in continuous miner machines), and so forth. In these cases, the EGVs are placed downstream and in close proximity of the fan to remove the swirl (flow rotation) to improve aerodynamic performance. The drawback is the increase in noise. Thus, the logical follow up research would be to investigate using multi-element airfoil on the EGVs for both as a noise reduction and aerodynamic improvement technology.
b) It was demonstrated that by simply turning off 2 out of the 7 fans (one fan was the closest to the ground) and operating them at higher speeds reduced the noise by nearly 6 dB while the net flow rate was increased by ~5%. Thus, it is suggested to investigate the impact of the fan-array distance to the ground on the noise and potentially the optimization of the large duct geometry. This investigation can be done numerically using CFD and then predicting the noise.
c) To advance the technologies investigated here, it is important to address cost issues. To this end, it is essential for university researchers to jointly work with the industry and government agencies (e.g. NIOSH) to find a path forward to implementation in the industry.

8. References:

Burdisso, R., Tarazaga, P. A., & Lee, J. (2017). *Low noise efficient rim driven auxiliary ventilation fans* (AFC215-21). Retrieved from

Cherniack, M., Brammer, A., Cavallari, J., & Peterson, D. (Producer). (2012). Noise and Vibration Related Disease in the Mining Industry. *Presentation to the Alpha Foundation for the Improvement of Mine Safety and Health, Inc*.

Chipperfield, A., & Fleming, P. (1995). The MATLAB genetic algorithm toolbox.

Drela, M. (2007). MSES 3.05: A multielement airfoil design analysis system. *A Research Program by: MIT Computational Aerospace Sciences Laboratory*.

Dwyer (Producer). (2016). Specifications-Installation and Operating instructions. Retrieved from https://www.dwyer-inst.com/PDF_files/122d.pdf

Hurtado, & Burdisso, R. (2018). *Low speed control vortex axial fan design for minimum noise.* Paper presented at the INTER-NOISE and NOISE-CON Congress and Conference Proceedings.

Hurtado, M., Wu, D., & Burdisso, R. (2017). Quiet rim driven ventilation fan design. *The Journal of the Acoustical Society of America, 141*(5), 3732-3732. doi:10.1121/1.4988196

Matetic, R., Randolph, R. F., & Kovalchik, P. G. (2012). Hearing Loss in the Mining Industry: The Evolution of NIOSH and Bureau of Mines Hearing Loss Research.

Yong-Han, K., Bo-Suk, Y., & Chang-Joon, K. (2006). Noise Source Identification of Small Fan-BLDC Motor System for Refrigerators. *International Journal of Rotating Machinery, 2006*. doi:10.1155/IJRM/2006/63214